Ultramicroscopy 111 (2011) 623–627

Contents lists available at ScienceDirect

Ultramicroscopy

journal homepage: www.elsevier.com/locate/ultramic

Pulsed-laser atom probe studies of a precipitation hardened maraging TRIP steel

O. Dmitrieva [a,*], P. Choi [a,*], S.S.A. Gerstl [b], D. Ponge [a], D. Raabe [a]

[a] Max-Planck-Institute for Iron Research, Max-Planck-Str. 1, 40237 Düsseldorf, Germany
[b] Imago Scientific Instruments, Madison, WI 53711, USA

ARTICLE INFO

Available online 15 December 2010

Keywords::
Pulsed-laser atom probe tomography
Local electrode atom probe
Microanalysis
Field evaporation
Precipitation hardened steels
Solute clustering

ABSTRACT

A precipitation hardened maraging TRIP steel was analyzed using a pulsed laser atom probe. The laser pulse energy was varied from 0.3 to 1.9 nJ to study its effect on the measured chemical compositions and spatial resolution. Compositional analyses using proximity histograms did not show any significant variations in the average matrix and precipitate compositions. The only remarkable change in the atom probe data was a decrease in the ++/+ charge state ratios of the elements. The values of the evaporation field used for the reconstructions exhibit a linear dependence on the laser pulse energy. The adjustment of the evaporation fields used in the reconstructions for different laser pulse energies was based on the correlation of the obtained cluster shapes to the TEM observations. No influence of laser pulse energy on chemical composition of the precipitates and on the chemical sharpness of their interfaces was detected.

1. Introduction

Over the past decade, there has been a rapidly growing interest in atom probe tomography (APT) as a technique for spatially resolved chemical analyses with near atomic resolution [1–8]. Recent developments in APT such as energy compensating wide angle reflectrons and ultrafast pulsed lasers have significantly improved the mass resolution and extended the applicability of this method to complex engineering alloys and materials with low electrical conductivity [1–8].

APT analyses of metallic samples have been traditionally carried out by applying high voltage pulses to the specimen with a typical pulse to base voltage ratio of about 20%. However, a common problem arising during voltage pulse APT analysis is premature specimen fracture. The exact mechanisms of this phenomenon remain unknown, but mechanical stresses associated with the high electric field at the specimen are believed to be its origin [9–11]. Pulsing with ultra-fast lasers has recently emerged as an attractive alternative to voltage pulsing. Laser pulsing offers certain advantages such as the capability of analyzing low-conductivity materials as well as an enhancement in mass resolution [4–6]. It has also been reported that laser pulsing leads to fewer specimen fractures due to a standing electric field, and thus constant mechanical stress applied to the specimen, whereas in the voltage mode the sample is exposed to a cyclically varying electric field. Moreover, the electric field is usually kept about 10–20% lower than for voltage pulsing [4]. However, the interaction between laser pulses and matter is not yet fully understood [12–16]. Temperature rises that occur during laser pulsing can deteriorate the spatial and mass resolution owing to surface diffusion and slow specimen cool-down [16,17]. Furthermore, standing field evaporation can occur for specimens of low thermal conductivity and low shank angle as a result of an increased specimen base temperature [16]. Ions that are field evaporated between the voltage/laser pulses are lost, which at best will lead to a reduction in the overall detection efficiency, and at worst lead to an error in composition measurement due to preferential evaporation of lower evaporation field elements. The studies of Sha et al. [18] and Vurpillot et al. [19] indicate that thermal effects are considered to play a major role in ion emission [18,19]. Vurpillot et al. [19] have shown that the observed fast anomalous cooling rate of the tip can only be related to a confined heating zone at the tip apex smaller than the wavelength of the laser.

Considerable effort has been put into the estimation of temperature rises during pulsed laser APT analyses and modeling the temperature profile [16–23]. A detailed work of Tang et al. [24] was performed on the influence of laser pulse energy on the mass resolution of APT [24]. However, in our work we investigated the influence of laser pulsing energy on the measured composition of complex precipitation-hardened alloy and on the chemical content and spatial detection of the intermetallic nano-precipitates. Compositional studies as a function of laser experiment parameters have been performed on selected Al- and Ni-based engineering alloys [25,26]. Laser energy dependent phenomena such as preferential evaporation, elemental surface diffusion, and local magnification could lead to deviations in the composition of the precipitates in complex steels. To our knowledge however, systematic pulsed laser

* Corresponding authors. Tel.: +49 211 6792325; fax: +49 211 6792333.
E-mail addresses: o.dmitrieva@mpie.de (O. Dmitrieva), p.choi@mpie.de (P. Choi).

0304-3991/$ - see front matter © 2010 Elsevier B.V. All rights reserved.
doi:10.1016/j.ultramic.2010.12.007

APT studies on steels still need to be done. In our previous work, we reported about a novel design approach for precipitation-hardened ductile high strength steels combining TRIP and maraging effects ("maraging TRIP steels") [27,28]. The addition of a few weight percent of Ni, Ti, and Al leads to the formation of nano-sized intermetallic precipitates in the martensitic FeMn matrix of these alloys, which can be detected by APT. Here we present and discuss the APT results obtained from analyzing this maraging TRIP steel, applying various laser pulse energies.

2. Experimental procedure

The alloy studied in this work contains 14 at% Mn, 5.3 at% Si, 5.5 at% Al, 0.6 at% Mo, and 1.8 at% Ni and balance Fe. Samples were subjected to a thermo-mechanical treatment process (as described in [27,28]) to ensure homogenization and removal of segregation. The aging treatment was conducted at 450 °C for 48 h. Transmission electron microscopy (TEM) (JEOL JEM 2200 FS operated at 200 kV) was performed to determine the precipitate size, morphology, and number density. APT measurements were carried out using a local electrode atom probe (LEAP^{TM} 3000X HR, Imago Scientific Instruments) equipped an ultrafast pulsed laser (~10 ps pulse width, 532 nm wavelength) with laser pulse energies between 0.3 and 1.9 nJ at a tip temperature of 50 K and a constant detection rate of 5 atoms per 1000 pulses. The laser pulse series was performed on the same tip except for the run done at 0.3 nJ. At least 20 million ions were collected in each run to reduce the statistical error. The APT data was evaluated with respect to the overall composition, precipitate size and composition (using the cluster search algorithm as described in [29–33]), and concentration across the interface between the matrix and the precipitates (using proximity histograms as described in [34]).

3. Results and discussion

3.1. Model reconstruction and estimation of evaporation fields

The observation of nanometer-sized precipitates by both APT and TEM allowed for proper adjustment of the APT reconstruction parameters using correlative microscopy. Spherical precipitates of a few nanometers in size were observed with TEM (Fig. 1). APT measurements were performed on the same sample (except for 0.3 nJ) at constant temperature (50 K). Therefore, to a first approximation the values for detector efficiency, geometrical field factor, and image compression factor were kept constant at 0.37, 3.3, and 1.65, respectively. The values for the evaporation field were varied until the reconstructions exhibited spherically shaped precipitates. These precipitates are enriched with Ni and Al (see Fig. 2a).

Fig. 3 shows the plot of the evaporation field F (chosen for proper reconstruction of the precipitates, correlated to TEM observations) vs. the laser pulse energy E_L. A nearly linear relationship between these two properties can be seen. The plot shows that with increase of the laser pulse energy, lower evaporation field is needed to achieve the same precipitate geometry (as observed by TEM) keeping the evaporation rate constant. It is widely accepted that the field evaporation process is predominantly thermally assisted for the laser parameters chosen in our work (~10 ps pulse width, 532 nm wavelength, 0.3–1.9 nJ laser pulse energy) [4,5,18,35]. It was found by Lee et al. [36] that the temperature rise of a tip having a long conical shank is proportional to the power of the illuminating focused beam of a laser operating at a range of wavelengths in the visible region of the spectrum [36]. Hence, our result is in good agreement with experimental observations made by Kellogg et al. [35,37], who found that the evaporation field of a tip decreases nearly linearly with the rising tip temperature.

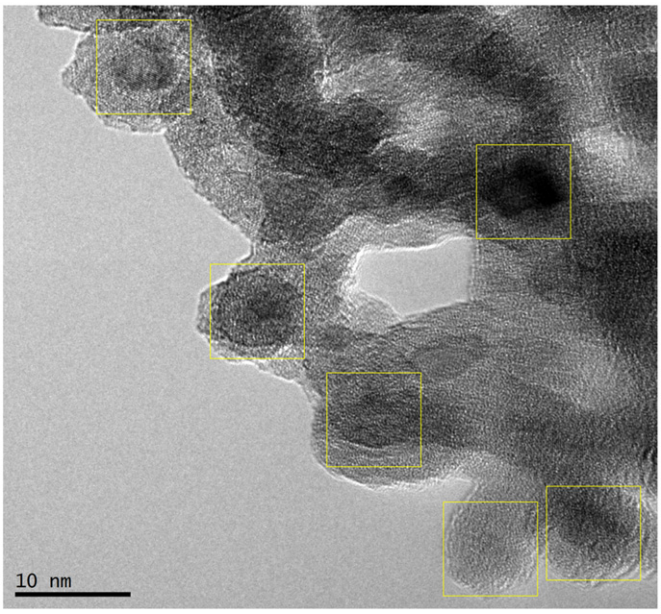

Fig. 1. TEM bright field image of the precipitation hardened steel sample. Spherically shaped particles of about 6 nm are observed.

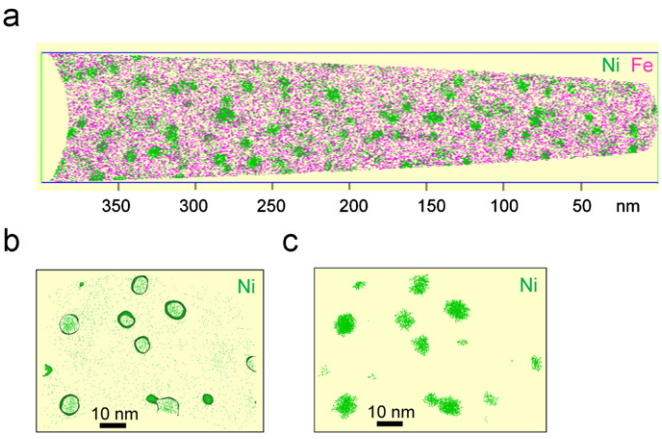

Fig. 2. (a) One of the reconstructions containing 62 million atoms (0.5 nJ analysis). Fe and Ni atoms are selected. (b) Cut through a reconstruction (for 1.3 nJ analysis) showing iso-concentration surfaces plotted at 9 at% Ni. (c) Cluster distribution obtained from the cluster search analysis (only Ni atoms are presented) performed for the run at 1.3 nJ. Cluster search parameters were $d_{max}=0.6$ nm, $N_{min}=50$, $L=0.55$ nm, and $d_{erosion}=0.50$ nm.

3.2. Study of elemental charge state ratios

The influence of the laser pulse energy on the charge state ratios (CSRs) of the alloy elements was studied. The intensity maxima of the most pronounced peaks of single charge and double charge ions in the mass spectrum were evaluated, where isotopes having no overlap with other elements were chosen. The CSRs of the isotopes $^{60}Ni^{++}/^{60}Ni^{+}$ and $^{55}Mn^{++}/^{55}Mn^{+}$ are plotted against the laser pulse energy in Fig. 3. Although the ++/+ CSRs are orders of magnitude different for Mn and for Ni ions (e.g., at 0.3 nJ, CSR is 3.3×10^{3} for Mn and 20 for Ni), a similar trend is found. The fraction of the doubly charged ions decreases drastically with increasing laser

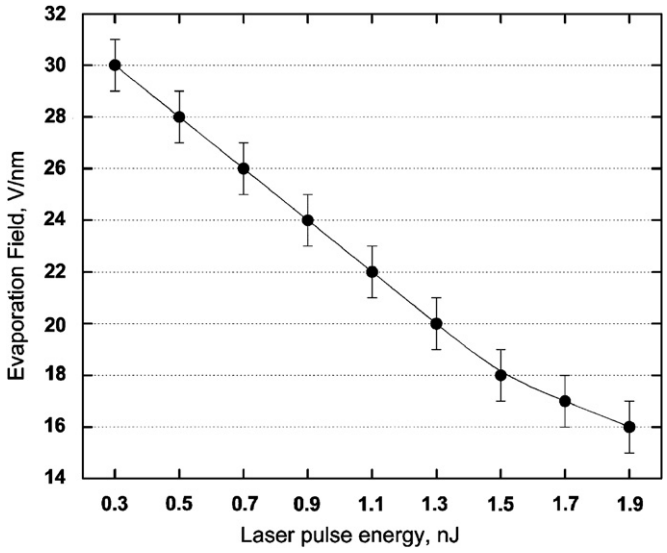

Fig. 3. Dependence of the mean evaporation field used for the reconstruction with the laser pulse energy in LEAP^{TM} 3000X HR done on the maraging TRIP steel sample.

energy and is smaller than 20% for laser energies above 1.1 nJ for Ni and 1.7 nJ for Mn. In contrast, the fraction of single charged ions increases with increasing laser pulse energy. These observations can be attributed to a rise in temperature during laser pulsing. Double or multiple charge states can be ascribed to post-ionization processes of single charged ions [39]. An increase in temperature must be accompanied by a decrease in activation energy Q for field evaporation if a constant evaporation rate is to be kept. The increase in Q is brought about by a decrease in electric field, as observed. Consequently, a lower electric field means less post-ionization and thus less doubly charged ions. A possible change in work function affects Q much less than the field and does not need to be considered.

3.3. Investigation of the total composition dependence on laser energy

The total compositions as measured by APT at various laser pulse energies were determined from mass spectra analyses. For analyses done at laser pulse energies ≥ 0.5 nJ a significant overlap of the $^{27}Al^{+}$ peak and $^{54}Fe^{2+}$ peak was observed, resulting in an increasing underestimation of the overall Al content. For these measurements the overall composition was corrected by applying a decomposition procedure for the overlapping mass peaks, which takes into account the isotope ratio of Fe. After the decomposition, nearly the same elemental composition was obtained for all laser pulse energies. The average measured compositions are 14.1 (± 0.1) at% Mn, 5.6 (± 0.3) at% Si, 5.7 (± 0.1) at% Al, 0.54 (± 0.05) at% Mo, and 2.4 (± 0.1) at% Ni, which correspond well to the nominal composition of the alloy. A slightly higher value for the Ni content (≈ 0.6 at%) in comparison to the nominal composition was detected for all laser energies. This difference can result from an inhomogeneous Ni distribution in the alloy on the micrometer scale.

3.4. Analysis of the precipitates using proximity histograms

In addition to the analysis of the total composition, a special emphasis was put on the analysis of the cluster contents. In the first step, the chemical composition of the precipitates can be analyzed by means of the proximity histogram (proxigram) as described in [34].

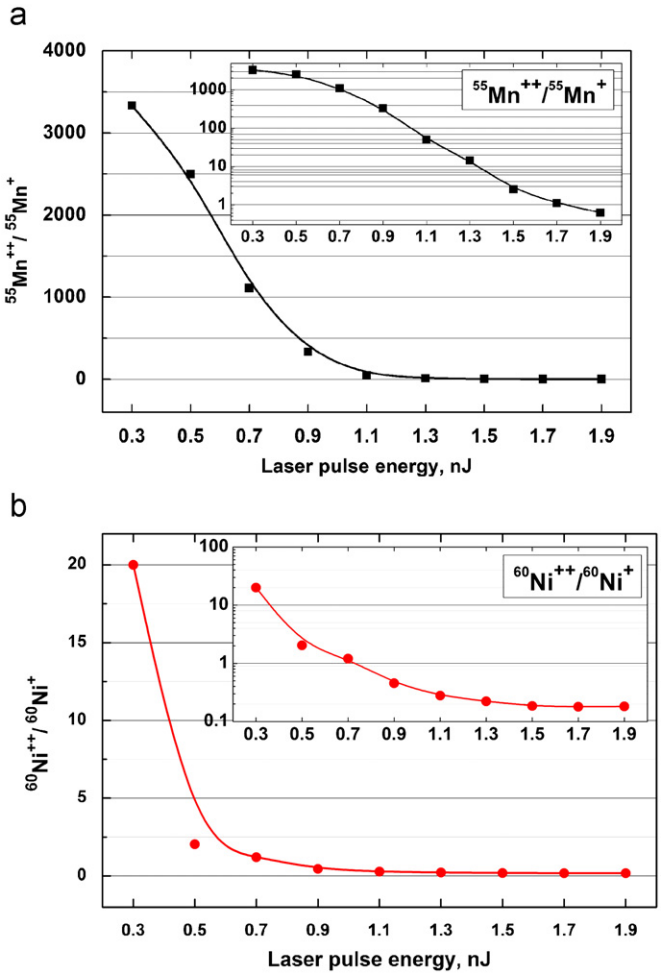

Fig. 4. Dependence the charge state ratios $^{60}Ni^{++}/^{60}Ni^{+}$ (a) and $^{55}Mn^{++}/^{55}Mn^{+}$ (b) on the laser pulse energy. In the insets, the charge state ratio values are logarithmic scaled.

Fig. 4 shows a proxigram averaged over all detected clusters (precipitates) for a laser pulse energy of 0.3 nJ. The major precipitation element is Ni (up to 45 at%) and Al (up to 25 at%). Diffuse chemical interfaces (about 2 nm in width) between the particles and the matrix are revealed in the proxigram. Slight enrichment of Si and Mn on the cluster interfaces is detected. Residual Fe and Mn contents (each about 15 at%) are found in the particle interior as well. This relatively large amount of Fe atoms in the clusters might be partly attributed to a local magnification effect since this well-known reconstruction artifact is particularly pronounced in heterogeneous materials and arises from differences in the evaporation field of the constituting phases or crystallographic planes [40–42]. Even though the values of the elemental evaporation fields are known (Fe 33, Mn 30, Ni 35, Al 19 V/nm), the sum and the interplay of the elemental evaporation fields in such an inhomogeneous alloy are hard to estimate. However, we did not detect any significant fluctuations in the total atomic density within the reconstruction, which indicates that this APT aberration might be not strongly developed in the investigated alloy. This means that a significant amount of Fe could be effectively present within the precipitates in this alloy (Fig. 5).

The influence of laser pulse energies on the sharpness of the interfaces between the precipitates and the matrix was studied in detail. Proxigrams for Ni, averaged over all detected precipitates, is plotted for various laser energies (Fig. 6). Ni was chosen, as it is enriched with a high content in the clusters providing good

statistics and, moreover, no significant peak overlap with other elements is detected. Interestingly, the proxigram slopes are nearly identical for all laser pulse energies. Some fluctuations observed within the proxigrams occur without any clear tendency related to the increase in the laser pulse energy and seem to be statistical. Even the detailed views presented in the insets reveal no dependence of the chemical gradients on the laser pulse energy. Scattering of the curves becomes larger on approaching the core of the precipitates, as the counting statistics deteriorate due to a decreasing number of sampled ions.

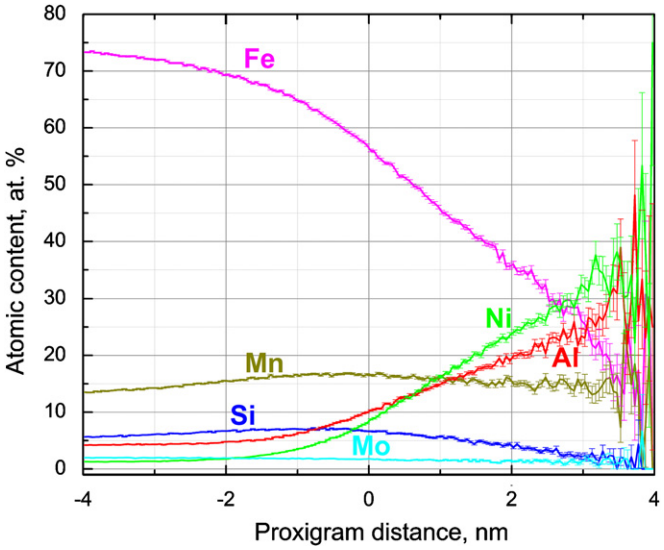

Fig. 5. Proximity histogram plotted for 0.3 nJ run and averaged over about 300 clusters. Iso-concentration surfaces were computed for the distance of ±4 nm from the position of the iso-surface at 8 at% Ni with the step size of 0.05 nm.

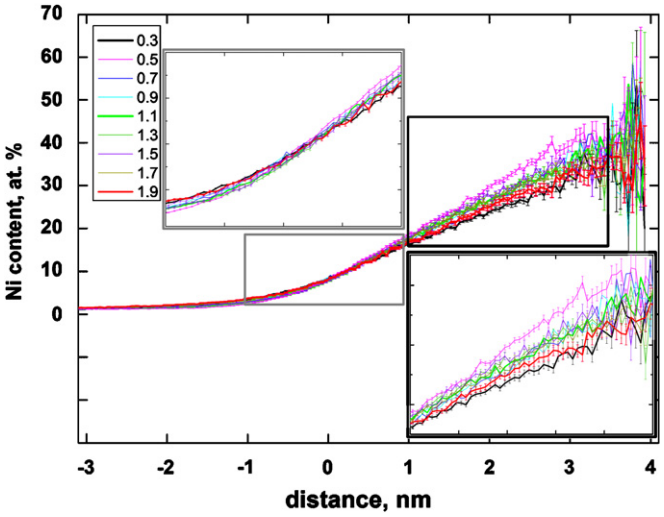

Fig. 6. Proxigram plotted only for Ni atoms computed for different laser energies. Surfaces were plotted at Ni 9 at% with step size 0.05 nm. In the insets, the enlarged views of two sections of the proxigram are shown.

3.5. *Study of the cluster contents as a function of different laser pulse energies*

Determination of the cluster sizes and their chemical contents as performed using a cluster search algorithm as described in Refs. [29–33]. The parameters used for the cluster search method are $d_{max}=0.6$ nm (maximal distance between the solute atoms belonging to the cluster), $N_{min}=50$ (minimal number for the solute atoms in the cluster), $L=0.55$ nm (envelope distance: all non-solute ions within L of solute ions are included in cluster), and $d_{erosion}=0.50$ nm (erosion distance: all clustered non-solute ions within $d_{erosion}$ of any ion outside of its assigned cluster are removed from the cluster). These values were determined via sequential standard analysis steps within the cluster search algorithm implemented in IVAS [29–33]. The cluster search was done for the distribution of Ni atoms. The clusters extracted from the reconstruction are shown in Fig. 2c (for laser pulse energy 1.3 nJ). The distribution of the clusters and morphology revealed by the cluster search procedure correspond to that observed in the iso-concentration surface plot (see Fig. 2b). The average cluster sizes and compositions determined from the cluster search analysis are listed in Table 1. It can be noticed that the cluster size remains constant within the statistical error with changing laser energies. Thus, the laser energy values in the studied range do not seem to have an influence on the local magnification of the clusters. The mean compositions of the clusters do not show any dependence on the laser energy and fluctuate statistically.

4. Conclusions

In this work, a precipitation hardened maraging TRIP steel was investigated using a pulsed laser atom probe. In the energy range from 0.3 to 1.9 nJ the measured overall composition of the alloy and the compositions of existing nano-precipitates were not affected by changes in the laser pulse energy, whereas the evaporation field and charge state ratios showed a strong dependence on the laser pulse energy. A decomposition of several overlapping mass-to-charge peaks was required to obtain an accurate composition of the alloy. The local magnification effect as well as preferential evaporation were not strongly dependent on the laser pulse energy. Also, no influence of the laser energy on the sharpness of the cluster interfaces was detected, which we associated with a weak contribution of the laser induced surface diffusion to that parameter.

Table 1
Mean cluster size and chemical content of the clusters obtained for the different laser pulse energies.

Laser pulse energy, *nJ*	**0.3**	**0.5**	**0.7**	**0.9**	**1.1**	**1.3**	**1.5**	**1.7**	**1.9**
Cluster size, nm	5.7 ± 2.1	5.9 ± 1.8	6.0 ± 2.2	5.9 ± 2.1	6.3 ± 1.4	6.1 ± 2.0	6.0 ± 1.9	5.9 ± 2.2	6.1 ± 2.1
Mean cluster content, at%									
Fe	38.5	35	36.8	36.9	36.6	36.1	37.2	38.3	39.5
Ni	25.1	24.7	23.5	23.8	24.3	24.7	24.8	24.4	23.6
Al	15.7	18.2	17	16.9	17.5	17.5	17.5	17.4	17.1
Mn	14.7	16.7	16.8	16.7	16.3	16.3	15.2	15.2	15.6
Si	5.6	5.6	5.6	5.3	5.0	5.1	4.9	4.4	3.9
Mo	0.4	0.3	0.3	0.3	0.3	0.3	0.3	0.3	0.3

References

[1] M.K. Miller, A. Cerezo, M.G. Hetherington, G.D.W. Smith, Atom Probe Field-Ion Microscopy, Oxford University Press, Oxford, 1996.
[2] M.K. Miller, Atom Probe Tomography—Analysis at the Atomic Level, Kluwer Academic/Plenum Publishers, New York, 2000.
[3] D. Seidman, Annu. Rev. Mater. Sci. 37 (2007) 127.
[4] T.F. Kelly, M.K. Miller, Rev. Sci. Instrum. 78 (2007) 031101.
[5] T.F. Kelly, D.J. Larson, K. Thompson, R.L. Alvis, J.H. Bunton, J.D. Olson, B.P. Gorman, Annu. Rev. Mater. Sci. 37 (2007) 681.
[6] A. Cerezo, P.H. Clifton, S. Lozano-Perez, P. Panayi, G. Sha, G.D.W. Smith, Microsc. Microanal. 13 (2007) 408.
[7] D. Blavette, E. Cadel, C. Pareige, B. Deconihout, P. Caron, Microsc. Microanal. 13 (2007) 464.
[8] M.K. Miller, R.G. Forbes, Mater. Charact. 60 (2009) 461.
[9] T.J. Wilkes, J.M. Titchmarsh, G.D.W. Smith, D.A. Smith, R.F. Morris, S. Johnston, T.J. Godfrey, P. Birdseye, J. Phys. D 5 (1972) 2226.
[10] S.V. Zaitsev, Tech. Phys. Lett. 30 (2004) 190.
[11] I.M. Mikhailovskij, N. Wanderka, V.E. Storizhko, V.A. Ksenofontov, T.I. Mazilova, Ultramicroscopy 109 (2009) 480.
[12] B. Gault, F. Vurpillot, A. Bostel, A. Menand, B. Deconihout, Appl. Phys. Lett. 86 (2005) 094101.
[13] A. Vella, F. Vurpillot, B. Gault, A. Menand, B. Deconihout, Phys. Rev. B 73 (2006) 165416.
[14] A. Vella, B. Deconihout, L. Marrucci, E. Santamato, Phys. Rev. Lett. 99 (2007) 046103.
[15] A. Cerezo, G.D.W. Smith, P.H. Clifton, Appl. Phys. Lett. 88 (2006) 154103.
[16] A. Cerezo, P.H. Clifton, A. Gomberg, G.D.W. Smith, Ultramicroscopy 107 (2007) 720.
[17] J.H. Bunton, J.D. Olson, D.R. Lenz, T.F. Kelly, Microsc. Microanal. 13 (2007) 418.
[18] G. Sha, A. Cerezo, G.D.W. Smith, Appl. Phys. Lett. 92 (2008) 043503.
[19] F. Vurpillot, J. Houard, A. Vella, B. Deconihout, J. Phys. D. 42 (2009) 125502.
[20] A. Cerezo, G.D.W. Smith, J. Phys. E 20 (1987) 1392.
[21] F. Vurpillot, B. Gault, A. Vella, M. Bouet, B. Deconihout, Appl. Phys. Lett. 88 (2006) 094105.
[22] A. Shariq, S. Mutas, K. Wedderhoff, C. Klein, H. Hortenbach, S. Teichert, P. Kücher, S.S.A. Gerstl, Ultramicroscopy 109 (2009) 472.
[23] E.A. Marquis, B. Gault, J. Appl. Phys. 104 (2008) 084914.
[24] F. Tang, B. Gault, S.P. Ringer, J.M. Cairney, Ultramicroscopy 110 (2010) 836.
[25] G. Sha, S.P. Ringer, Ultramicroscopy 109 (2009) 580.
[26] Y. Zhou, C. Booth-Morrison, D. Seidman, Microsc. Microanal. 13 (2008) 571.
[27] D. Raabe, D. Ponge, O. Dmitrieva, B. Sander, Adv. Eng. Mater. 11/7 (2009) 547.
[28] D. Raabe, D. Ponge, O. Dmitrieva, B. Sander, Scr. Mater. 60 (2009) 1141.
[29] L.T. Stephenson, M.P. Moody, P.V. Liddicoat, S.P. Ringer, Microsc. Microanal. 13 (2007) 448.
[30] A. Cerezo, L. Davin, Surf. Interface Anal. 39 (2–3) (2007) 184.
[31] M.K. Miller, E.A. Kenik, Microsc. Microanal. 10 (3) (2004) 336.
[32] D. Vaumousse, A. Cerezo, P.J. Warren, Ultramicroscopy 95 (2003) 215.
[33] M.P. Moody, L.T. Stephenson, A.V. Ceguerra, S.P. Ringer, Microsc. Res. Tech. 71 (2008) 542.
[34] O.C. Helman, J.V. Vandenbroucke, J. Rüsing, D. Isheim, D.N. Seidman, Microsc. Microanal. 6 (2000) 437.
[35] G.L. Kellogg, T.T. Tsong, J. Appl. Phys. 51 (1980) 1184.
[36] M.J.G. Lee, R. Reifenberger., E.S. Robin, H.G. Lindenmeyr, J. Appl. Phys. 51 (9) (1980) 4996.
[37] G.L. Kellogg, J. Appl. Phys. 52 (1981) 5320.
[39] D.R. Kingham, Surf. Sci. 116 (1982) 273.
[40] M.K. Miller, M.G. Hetherington, Surf. Sci. 61 (1991) 442.
[41] D. Blavette, F. Vurpillot, P. Pareige, A. Menand, Ultramicroscopy 89 (2001) 145.
[42] F. Vurpillot, A. Bostel, D. Blavette Appl., Phys. Lett. 76/21 (2000) 3127.